Online ISSN: 2981-0396 Print ISSN: 2981-0388

International Journal of Iron & Steel Society of Iran

Journal Homepage: https://journal.issiran.com/

Research Article

Fabrication of CK45/RGO Nanocomposite Using Machining Chips Recycling and Spark Plasma Sintering

S. M. R. Sedehi *[1], S. H. Yazdi [2], Z. Bazleh [3], M. Boskabadi [4], A. Sistani [5]

[1] *Faculty of Mechanical Engineering, Technical Campus, University of Tehran, Tehran, Iran*
[2,3,4,5] *Aseman Nano Part Company, Gonabad, Iran*

ARTICLE INFO

Keywords:

Steel, Reduced Graphene Oxide, Chip, Recycling, Machining, Spark Plasma Sintering.

Article history:

Received 13 February 2024
Received in revised form 20 May 2024
Accepted 31 August 2024

ABSTRACT

Recycling approaches are emerging as intriguing and sustainable topics for environmental safety. Machining chips offer the possibility of reuse in more sustainable and cost-effective production pathways, such as producing powder from milled scraps for additive manufacturing. Recycling practical materials like steel with low processing costs, combining economic and engineering advantages, presents a vital demand for designing more sustainable and reliable components for the aerospace and automotive industries. The present study utilizes CK45 steel for recycling and, by generating machining scraps in a closed-loop cycle, achieves a unique combination of material properties. The produced composites containing 0.1% and 0.2% weight percentages of reduced graphene oxide are fabricated using spark plasma sintering. They undergo hardness, compression, wear, and corrosion tests, as well as scanning electron microscopy (SEM) and XRD analysis for comprehensive characterization. Hardness and wear tests reveal that these waste materials possess suitable hardness for use in parts manufacturing for industries in which the Hardness and wear resistance are important factors in service conditions. The results of hardness and wear investigations indicate an increase in hardness by 140 units and a weight reduction of 18 mg in the produced samples compared to the cast sample.

1. Introduction

Industrial activity in 2021 directly accounted for the emission of 9.4 gigatons of carbon dioxide (CO_2), constituting a quarter of global emissions, with iron and steel production contributing to 30% of the world's CO_2 emissions in 2021 [1]. This trend is on the rise, as industrial emissions have increased by over 70% from 2000 to the present, driven by the growing global demand for industrial goods coupled with marginal improvements in energy efficiency [1]. It is easily foreseeable that decoupling material demand from economic and population growth can contribute to reducing CO_2 emissions. One of the primary paths to reduce primary material production and resource extraction from economic growth involves implementing circular economy strategies, including longer product lifetimes, repairability, product upgrades, modularity, remanufacturing, and material reuse and recycling. Solid-state recycling strategies are one of the methods that can prevent damage to recycled production components. This method directly transforms steel scrap into semi-finished products, avoiding the remelting stage completely. In

*Corresponding author
Email: mrsedehi@ut.ac.ir
Address: Faculty of Mechanical Engineering, Technical Campus, University of Tehran, Tehran, Iran
1.Ph.D. Candidate, 2. M. S., 3. M. S., 4. M. S., 5. M. S.

DOI: http://10.22034/IJISSI.2024.2022975.1280
Published by ISSI (Iron & Steel Society of Iran)

environments where access to raw materials and energy consumption are crucial factors, the ability to harvest metal waste and reuse it as raw materials can facilitate production during times when material availability is limited. Utilizing powder obtained from machining chips has been explored in the past [2]. In general, chips produced by machining processes are considered metal waste and are sent for melting, completely erasing their processing history. In a recent study, a repetitive process approach was followed for producing cylinders by compacting tool steel AISI-SAE H11 machining chips, which had previously been transformed into powders [3]. Effectively, metal chips, rather than adhering to a thermomechanical route, can serve as raw materials for powder technologies like additive manufacturing (AM) [4]. Additive manufacturing is a concept for a broad spectrum of emerging production methods based on the application of powder for producing components, involving three stages powder chip production, filtration, and welding. It is noteworthy that such processing is currently one of the most common production methods [5]. One sustainable processing method with the capability to process various metals is the powder metallurgy method, which can make the value of recycled machining chips more significant. In the field of metal composites produced by spark plasma sintering, rejuvenated graphene oxide is used as a reinforcement and is often employed to improve mechanical properties [6]. In recent years, powder metallurgy processing has gained increasing application due to its numerous advantages compared to other production processes. The ability for further alloying and good self-lubricating properties, along with economical fabrication of complex-shaped machine elements, are among these advantages [7]. Besides the usual benefits, powder metallurgy steels have better microstructural properties, such as homogeneity in carbide distribution in the matrix and smaller grain sizes compared to regular steels. Therefore, some powder metallurgy steels with low porosity and high wear resistance, particularly for parts with wear like gears and bearings, have found widespread applications in the automotive industry, in engines, and in transmission systems [9, 8]. In recent years, the mechanical properties of porous steels have been primarily studied through tensile and impact testing [10]. However, the demand for producing parts under heavy mechanical loads and complex forces, such as engine and transmission gears, requires dynamic properties such as wear and fatigue behavior of porous materials to be studied [11, 12]. Fatigue and wear phenomenon are the two main reasons for engineering component failure that start from or near the surface. The initiation of core crack begins from near-surface pores and propagates through inter-pore ligaments. The fatigue life also decreases with an increase in total porosity [13]. On the other hand, in recent years, graphene, which has considerable electrical and thermal conductivity [14], high Young's modulus [15], and desirable tensile strength [16], has been utilized in various applications for producing different nanocomposites due to its unique properties such as tensile strength up to 200 times that of steel, susceptibility to form hard phases, and excellent wear resistance [17].

2. Materials and experimental procedures

2.1. Machining and Chip Formation

Steel chips were produced from CK45 round bars using a closed-loop machining cycle with the parameters listed in Table 1. and depicted in Fig. 1. It is noteworthy that the machining process was performed at an industrial production center, and the cutting parameters presented in Table 1. are part of common industrial machining practices. It is essential to ensure that the characteristics of the chips used in this work are somewhat representative of the chips produced in the industrial manufacturing of components.

2.2. Production of Reduced Graphene Oxide (RGO)

Graphene oxide was prepared through a modified Hummers method from the initial graphite powder [18]. A 200 ml aqueous solution of graphene oxide with a concentration of 5.2 mg/ml was prepared and subjected to ultrasonic waves for 1 h to achieve dispersion. For reduction, the suspension was placed inside an autoclave under hydrothermal conditions for 12 h at a temperature of 190 ℃ and a pressure of 12 bar. Subsequently, the obtained hydrogel product underwent a freeze-drying process at -50 ℃ for 12 h to remove absorbed water from its surface and form a porous network structure [19].

Table 1. machining parameters.

Parameter	Value
Feed rate (mm)	0.1
cutting depth (mm)	0.5
Tooltip radius (mm)	0.1
Cutting tool rotation (rpm)	350
Cooler	-

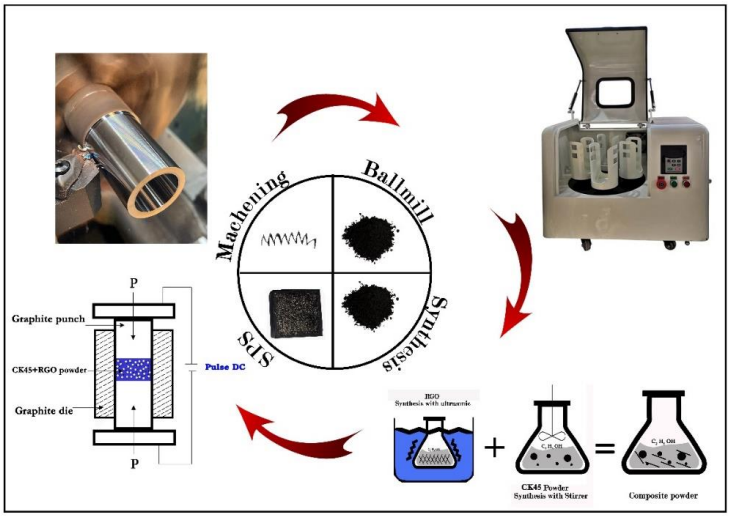

Fig. 1. Schematic of the process.

2.3. Combination of Powders and Characterization of Composite Samples

To achieve a uniform blend of the final composite powder, CK45 chips and RGO powder were mixed in a ball mill for 3 h under the conditions specified in Table 1. and Fig. 1. using argon gas as a protective atmosphere. Subsequently, for powder compression and the production of test specimens using the spark plasma sintering (SPS) method, a graphite mold with an internal diameter of 20 mm was used. A graphite foil with a thickness of 0.5 mm was placed between the mold and the powder to create a uniform current in the powder and prevent contamination of the produced sample. This process was carried out with a heating rate of 50 °C/min, holding time of 6 min, and low and high pulses of 40 and 200 microamperes per second, respectively. The pressure and temperature were set at 45 megapascals and 850 °C, respectively. SEM images of the initial samples and the produced samples are shown in Fig. 2. Fig. 2-a. illustrates the microstructure of the CK45 steel base metal, showing a ferritic structure in dark color and a martensitic structure in light color. The presence of graphene in the sample is evident in Fig. 2-b. showing a well-defined bond and material structure. The sample without graphene also exhibits fractures on the surface, significantly affecting the mechanical properties. After producing the samples, cross-sectional parts perpendicular to the pressing direction were examined using a Meiji inverted metallographic microscope. To reveal the sample surfaces, a chemical solution with a composition of 1-5% HNO_3, 65-75% H_3PO_4, and 5-10% CH_3COOH was used. Subsequent experiments aimed to further investigate the phases present in the samples using X-ray diffraction (XRD) with an Explorer device by GNR Italy under the conditions of V=40Kv and Current = 30mA. Morphological changes in the welded samples were examined using a field emission scanning electron microscope (FE-SEM) model MIRA3 by TESCAN, Czech Republic, with a resolution of 1.5 nm at a voltage of 15 kV. The hardness of the samples was measured using a Vickers method with an INNOVATEST NEXUS 8000XL hardness tester, applying a 9.612 N load with a tungsten carbide indenter of 2.5 mm in diameter and holding for 15 sec. according to ASTM A370 (2020) standard. To obtain the average mean, each sample was tested a minimum of 3 times. Wear tests were conducted using a pin-on-disk method in a specialized laboratory according to ASTM G99 standard at room temperature under dry conditions, with a force of 5 N, a time of 3600 sec, and a speed of 60 revolutions per minute using a steel pin as the slider. Electrochemical corrosion tests on the samples were performed in a voltage range of -250 to +250 mv, a scan rate of 1 mv, and an open circuit potential (OCP) time of 1200 sec.

3. Results and discussion

3.1. Microstructure of light microscope

The size and shape of grains are among the most crucial factors influencing the properties and behavior of metals. It is well-known that the mechanical, chemical, biological properties, superplastic behavior at high temperatures, corrosion behavior, and many other characteristics of metals depend on the conditions of microstructure and grain size [20]. The results related to grain size in the metallographic test of the fabricated samples are shown in Fig. 3. As the results indicate, with the refinement of grains acc. to Figs. 3-a-b and c. in the structure of the produced samples, the grain boundaries increase, and the corrosion resistance decreases to the same extent. However, the phenomenon of grain refinement leads to an increase in mechanical properties, including compressive strength, hardness, and wear resistance.

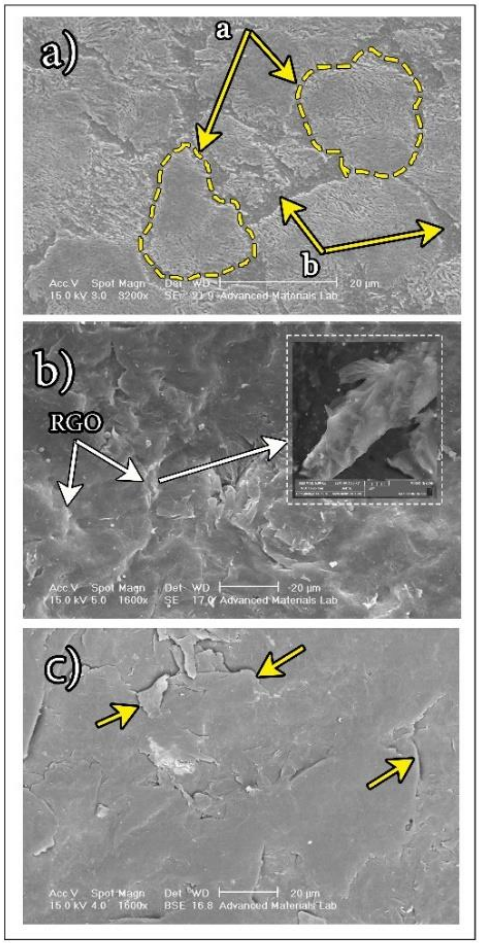

Fig. 2. SEM Images of a) CK45 Cast Sample, b) RGO/CK45 Sample, c) Sample Without RGO.

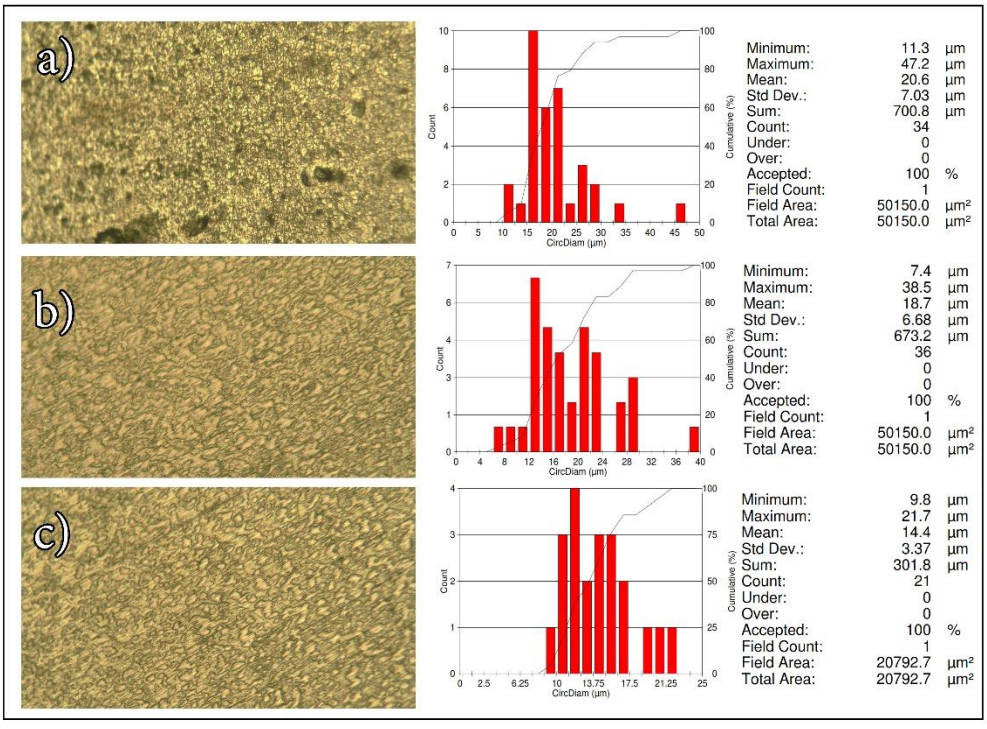

Fig. 3. Microstructural metallographic results.

3.2. Investigation of CK45/RGO composite with X-ray diffraction (XRD)

To investigate the changes in phases during the three machining processes, ball milling, and SPS, XRD analysis was performed on the samples. In Fig. 4. the XRD pattern is presented. According to the obtained results, it was found that no phase changes occurred in the samples during the milling process, which is evidence of the successful completion of this stage. However, in the ball milling stage, the possible chemical composition of the produced powder affected the diffraction peaks, leading to the observation of peaks at 200 and 220. In the XRD patterns of the composite samples after SPS, a weak peak at 26.5 degrees corresponding to RGO was observed. Also, the absence of a carbide phase in the samples produced by SPS is attributed to the proper control of manufacturing conditions and prevention of carbon infiltration in this method. In XRD analysis, the broadening of the highest peak is mainly attributed to the small size of grains and lattice distortion [21], which is clearly evident in this study and in the samples after ball milling.

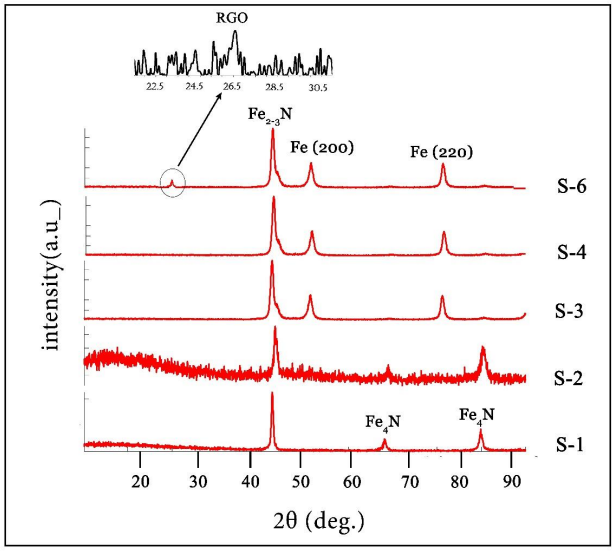

Fig. 4. XRD micrographs of the pure sample, chip, and CK45/RGO composite.

3.3. Compression Test

In Fig. 5. the stress-strain curves at different stages of the experiments are presented. According to the well-known Hall-Petch equation shown below, grain refinement enhances the strength of the structure [22]. This is evidenced by the decrease and increase in yield and ultimate strength, respectively, for both annealed and one-pass simple shear extrusion. In the Hall-Petch equation, σ_y is the yield stress, σ_0 is the yield stress of a polycrystalline material with infinite grain size (hypothetical single crystal with random orientation), k is the locking parameter or patch parameter (material constant), and d is the average grain diameter [23]:

$$y = \sigma_0 + \frac{K}{\sqrt{d}}\sigma \qquad \text{Eq. (1)}$$

Another factor contributing to the increased strength in ultrafine-grained materials is strain hardening. The density of dislocations, new grain boundaries, and voids increase with the sintering process, and the multiplication of these defects in the material leads to an increase in strain hardening. The hydrostatic pressure present in this method significantly influences the strength enhancement of ultrafine-grained materials. The concentration of voids during plastic deformation increases due to this type of pressure, and the penetration of dislocations into voids becomes more difficult. As a result, the void elimination process slows down, and ultimately, the strain hardening rate increases with the reduction in the processing speed of voids [24]. Based on the results obtained in Fig. 5. it is quite evident that adding RGO nanoparticles has a significantly positive effect on the compressive strength performance of the produced specimens. Another interesting and important result of the compression test is the optimum amount of carbon reinforcement, where increasing the percentage of reinforcement from 0.01 to 0.02 W% leads to a decrease in compressive strength.

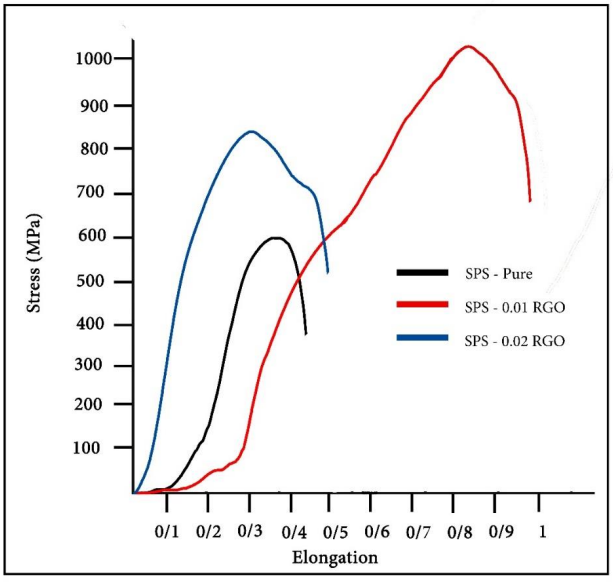

Fig. 5. Compression test results.

3.4. Microhardness

The obtained values after Vickers microhardness testing on samples produced at various stages are presented in Fig. 6. The hardness levels of the produced samples with recycled powder from CK45 steel chips confirm the rationality of the test procedures in the direction of this

mechanical property. As visible in this figure, the Vickers hardness number of 218 for the cast sample, respectively for samples with 0%, 0.1%, and 0.2% by weight of RGO after the SPS process, not only confirms the increased hardness of the chips separated from the material compared to the initial substance, but also highlights the effectiveness of the RGO on the material's hardness. On the other hand, the enhancement of hardness in the samples can also be related to grain size. As indicated in the metallography results, the grain size exhibited a decreasing trend for the first, second, and third samples, respectively.

3.5. Wear Behavior

In this test, the impact of composite formation through the recycling of machining chips and the use of RGO as a reinforcement in samples produced by the SPS method has been evaluated. Fig. 7. illustrates the weight loss of test samples in terms of the distance traveled compared to pure CK45 steel cast samples. As evident in the figure, the wear rate of the cast sample is generally much higher than the samples produced with recycled powder from CK45 steel machining chips. Regarding the presence of RGO in the samples, it can be noted that its positive presence optimally affects the wear rate, and exceeding that threshold leads to a reduction in wear resistance. This aligns with the hardness results related to the extracted grain size from metallography, indicating a specific correlation with grain size in the wear test as well. Summarizing the issues related to grain size and the presence of RGO, it can be concluded that the reduction in wear resistance in the third sample is solely due to the amount of RGO. according to the results and explanation above a correlation between wear and hardness results based on the Hall-Petch law, both test results should be similar. On the other hand, Taheri et al., [25] in their research, attributed this phenomenon to the agglomeration (sticking together) of nano-plates in the sample with a very high amount of RGO, suggesting a potential decrease in properties. The results of the wear test suggest that the second sample, which has the best performance, showed a decreasing or constant trend in all stages of this test, while other samples exhibited oscillations. As mentioned in the previous explanations, due to the increase in hardness and wear resistance in the machined scrap compared to the base metal, these property enhancements have also been transferred to the produced specimens.

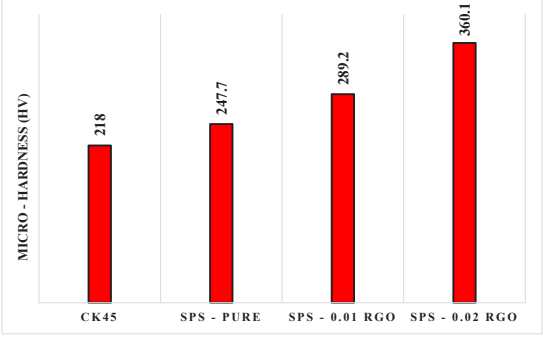

Fig. 6. Vickers hardness test results.

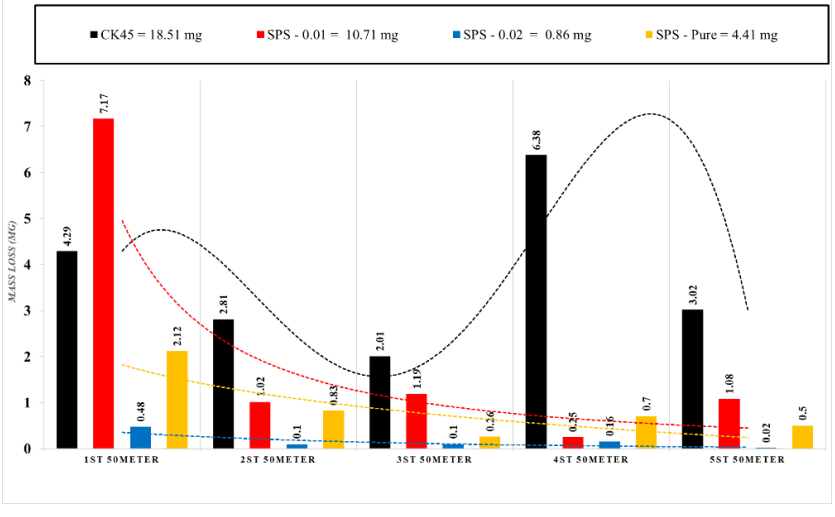

Fig. 7. Weight Loss of Samples during Wear Test.

3.6. Corrosion Test

To measure corrosion, Tafel slopes were plotted in the linear region of polarization curves, and the polarization resistance was calculated based on the Stern–Geary equation, as stated below [26]:

$$R_P = \frac{b_a b_c}{2.303(b_a+b_c)i_{corr}} \quad \text{Eq. (2)}$$

$$i_{corr} = \frac{B}{R_P} \quad \text{Eq. (3)}$$

$$B = \frac{b_a b_c}{2.303(b_a+b_c)} \quad \text{Eq. (4)}$$

In which R_p is the linear polarization resistance (LPR) of the coating, b_a and b_c are the Tafel slopes of the anodic and cathodic branches, respectively. i_{corr} is the corrosion current density, and E_{corr} is the corrosion potential. These parameters and the corrosion rate for the produced samples compared to the pure cast CK45 sample are presented in Table 2. and Fig. 8. According to the data extracted from the Stern–Geary equation [26], the corrosion potential has been converted from -28 mV in the cast sample to higher values in the sintered samples, indicating a shift of potential to less noble values and an increased likelihood of thermodynamic corrosion in these samples [25]. Moreover, the corrosion current density has decreased from 73 to 10 μA/cm² in the sample with the least amount of RGO. Due to composite formation in the sample containing 0.01 w% RGO, the corrosion current has decreased more than 7 times compared to the cast sample. With the addition of RGO, the corrosion resistance relative to the pure sintered sample has decreased, According to past researchers' opinions, the most important reason for this phenomenon could be the aggregation of RGO nanoplatelets during the manufacturing processes [25]. Research has shown that if the corrosion potential increases and the corrosion current density decreases, the corrosion of the sample decreases [27], which has been recorded in cast and sintered samples.

4. Conclusions

In the current research, CK45 steel was used for scrap recycling, and by creating a closed cycle, it was possible to achieve a rare combination of material characteristics. Production composites containing 0, 0.01 and 0.02 weight percent of RGO were made by spark plasma sintering method and subjected to hardness, tensile, wear, corrosion, and scanning electron microscope and XRD tests for their properties. And the following results have been obtained:

- Hardness and wear tests have shown that this type of waste has suitable hardness to be used in parts making in industries sensitive to hardness and wear.
- The numerical values of the hardness and wear test show the growth of 140 units of hardness and a decrease of 18 mg in the weight of the production samples compared to the cast prototype.
- Additionally, the compressive strength of the produced specimens increases after the addition of RGO reinforcement compared to the pure specimen. This increase in compressive strength is optimum for the weight percentage of the reinforcement, and after that, the compressive strength decreases again.

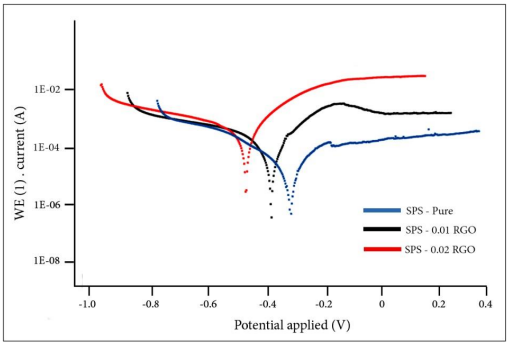

Fig. 8. The potentiodynamic polarization test curves.

Table 2. Corrosion Test Results.

	CK45	SPS - Pure	SPS – 0.01 RGO	SPS – 0.02 RGO
E_{corr} (V)	-0.028	-0.352	-0.417	-0.503
i_{corr} (A)	73	34	10	31
b_a (V/dec)	0.062	0.092	0.085	0.099
b_c (V/dec)	0.182	0.103	0.110	0.160
R_p (ohm)	537.8	6132	1962.1	855.62
Corrosion rate (mm/year)	0.077	0.01	0.032	0.095

- The corrosion results also indicate that specimens produced from recycled CK45 steel scrap have higher corrosion resistance compared to the cast specimen of this metal. The best condition is observed for the pure specimen, and after adding the highest percentage of weight of reduced graphene oxide, due to the aggregation of nanoparticles, the corrosion resistance is even lower than that of the cast specimen.

Reference

[1] Puleo R, Latif A, Ingarao G, Di Lorenzo R and Fratini L, Solid bonding criteria design for aluminum chips recycling through Friction Stir Consolidation, Journal of Materials Processing Technology. 2023; 319: 118080.
[2] Beck S.C, Williamson C.J, Kinser R.P, Rutherford B.A, Williams M.B, Phillips B.J, Doherty K.J, Allison P. G and Jordon J.B, Examination of microstructure and mechanical properties of direct additive recycling for Al-Mg-Mn alloy Machine chip waste, Materials & Design. 2023; 228: 111733.
[3] Bhatta G, Valladares L, Liu X, Ma Z, Domínguez A.B, Moreno N.O, Suarez S.E, Barnes C.H.W, Zhang D, Microstructure and mechanical properties of solid state recycled 4Cr5MoSiV (H11) steel prepared by powder metallurgy, Res. Mater. 2021; 100184.
[4] Santos R.F, Farinha A.R, Rocha R, Batista C, Costa Rodrigues G, Vieira M.T, High-speed machining tool-steel chips as an outstanding raw material for indirect additive manufacturing? Results in Materials. 2021; 11: 100207.
[5] Hahn E.N, Meyers M.A, Grain-size dependent mechanical behavior of nanocrystalline metals. Mat Sci Eng A-Struct. 2015; 646: 101–134.
[6] Sedehi S.M.R, Khosravi M, Yaghoubinezhad Y, Mechanical properties and microstructures of reduced graphene oxide reinforced titanium matrix composites produced by spark plasma sintering and simple shear extrusion. Ceramics International. 2021; 47(23): 33180-33190.
[7] Dhanasekaran S, Gnanamoorthy R, Abrasive wear behavior of sintered steels prepared with MoS2 addition. Wear. 2007; 262(5-6): 617-623.
[8] Hortenhuber A, PM camshaft technology, Met Powder Rep. 1992; 47(1): 16-19.
[9] Babakhani A, Haerian A, Ghambri M, Effect of heat treatment, lubricant and sintering temperature on dry sliding wear behavior of medium alloyed chromium PM steels, Journal of Materials Processing Technology. 2008; 204(1-3): 192-198.
[10] Hausner H.H, Mal K, Handbook of Powder Metallurgy, New York: Chemical Publications; 1982.
[11] Danninger H, Spoljaric D, Weiss B, Microstructural features limiting the performance of PM steels, International Journal of Powder Metallurgy. 1997; 33(4): 43-53.
[12] Lim S.C, Lim C.Y.H, Lee K.S, The effects of machining conditions on the flank wear of TiN-coated high speed steel tool inserts. Wear. 2002; 181-183(2): 901-912.
[13] Khorsand H, Habibi S.M, Yoozbashizadea H, Janghorban K, Reihani S.M.S, Rahmani Seraji H, Ashtari M, The role of heat treatment on wear behavior of powder metallurgy low alloy steels. Materials and Design. 2002; 23(7): 667-670.
[14] Balandin A.A, Ghosh S, Bao W, Calizo I, Teweldebrhan D, Miao F, et al. Superior thermal conductivity of single-layer graphene. Nano Lett. 2008; 8(3): 902-907.
[15] Novoselov K.S, Geim A.K, Morozov S.V, Jiang D, Zhang Y, Dubonos S.V, et al. Electric field effect in atomically thin carbon films. Science. 2004; 306(5696): 666-669.
[16] Lee C, Wei X, Kysar J.W, Hone J, Measurement of the elastic properties and intrinsic strength of monolayer graphene, Science. 2008; 321(5887): 385-388.
[17] Liu L, Zhou M, Jin L, Li L, Mo Y, Su G, et al. Recent advances in friction and lubrication of graphene and other 2D materials: Mechanisms and applications, Tribol Int. 2019; 7:199-216.
[18] Hummers Jr W.S, Offeman R.E, Preparation of graphitic oxide, J Am Chem Soc. 1958; 80(6): 1339.
[19] Jia H, Xu J, Lu L, Yu Y, Zuo Y, Tian Q, et al. Three-dimensional Au nanoparticles/nano-poly (3,4-ethylene dioxythiophene)-graphene aerogel nanocomposite: a high-performance electrochemical immunosensing platform for prostate specific antigen detection, Sensor Actuator B Chem. 2018; 260: 990-997.
[20] Langdon T.G, The processing of ultrafine-grained materials through the application of severe plastic deformation. J Mater Sci. 2007; 42: 3388-3397.
[21] Liu J, Liang C, Microstructure characterization and mechanical properties of bulk nanocrystalline aluminium prepared by SPS and followed by high-temperature extruded techniques, Materials Letters. 2017; 206: 95-99.
[22] Sergueeva A.V, Stolyarov V, Valiev R, Mukherjee A.K, Advanced Mechanical Properties of Pure Titanium with Ultrafine Grained Structure, Scripta Materialia. 2001; 45(7): 747-752.
[23] Phaniraj M.P, Prasad M.J.N.V, Chokshi A.H, Grain-Size Distribution Effects in Plastic Flow and Failure, Materials Science and Engineering: A. 2007; 463(1-2): 231-237.
[24] Torabzadeh H, Faraji G, A Review of the Production of Ultrafine Grained and Nanograined Metals by Applying Severe Plastic Deformation. Modares Mechanical Engineering. 2016; 16(6): 271-282.
[25] Taheridoustabad I, Khosravi M, Yaghoubinezhad Y, Fabrication of GO/RGO/TiC/TiB2 nanocomposite coating on Ti–6Al–4V alloy using electrical discharge coating and exploring its tribological properties, Tribology International. 2021; 156: 106860.
[26] Cheng L, Liu C, Han D, Ma S, Guo W, Cai H, et al. Effect of graphene on corrosion resistance of waterborne inorganic zinc-rich coatings, Journal of Alloys and Compounds. 2019; 774: 255-264.
[27] Zhang Y, Chen F, Zhang Y, Du C, Influence of graphene oxide additive on the tribological and electrochemical corrosion properties of a PEO coating prepared on AZ31 magnesium alloy. Tribology International. 2020; 146: 106135.